High-resolution forest carbon stocks and emissions in the Amazon

Gregory P. Asner[a,1], George V. N. Powell[b], Joseph Mascaro[a], David E. Knapp[a], John K. Clark[a], James Jacobson[a], Ty Kennedy-Bowdoin[a], Aravindh Balaji[a], Guayana Paez-Acosta[a], Eloy Victoria[c], Laura Secada[d], Michael Valqui[d], and R. Flint Hughes[e]

[a]Department of Global Ecology, Carnegie Institution for Science, Stanford, CA 94305; [b]World Wildlife Fund, Washington, DC 20090; [c]Peruvian Ministry of Environment, Lima 27, Peru; [d]World Wildlife Fund, Lima 14, Peru; and [e]Institute of Pacific Islands Forestry, United States Forest Service, Hilo, HI 96720

Edited by B. L. Turner, Arizona State University, Tempe, AZ, and approved August 10, 2010 (received for review April 9, 2010)

Efforts to mitigate climate change through the Reduced Emissions from Deforestation and Degradation (REDD) depend on mapping and monitoring of tropical forest carbon stocks and emissions over large geographic areas. With a new integrated use of satellite imaging, airborne light detection and ranging, and field plots, we mapped aboveground carbon stocks and emissions at 0.1-ha resolution over 4.3 million ha of the Peruvian Amazon, an area twice that of all forests in Costa Rica, to reveal the determinants of forest carbon density and to demonstrate the feasibility of mapping carbon emissions for REDD. We discovered previously unknown variation in carbon storage at multiple scales based on geologic substrate and forest type. From 1999 to 2009, emissions from land use totaled 1.1% of the standing carbon throughout the region. Forest degradation, such as from selective logging, increased regional carbon emissions by 47% over deforestation alone, and secondary regrowth provided an 18% offset against total gross emissions. Very high-resolution monitoring reduces uncertainty in carbon emissions for REDD programs while uncovering fundamental environmental controls on forest carbon storage and their interactions with land-use change.

deforestation | forest degradation | Peru | Reduced Emissions from Deforestation and Degradation | United Nations Framework Convention on Climate Change

Between 10% and 15% of global carbon dioxide emissions originate from deforestation and degradation of tropical forests (1, 2). Emblematic of these emissions, the southwestern Peruvian Amazon is undergoing carbon changes via road building, mining, timber extraction, and farming. Meanwhile, the United Nations Framework Convention on Climate Change is working to develop a program to curb carbon emissions via the program for Reduced Emissions from Deforestation and Degradation (REDD) (3, 4). REDD has the potential to connect carbon emitters with governments positioned to reduce forest carbon losses through monetary compensation. In addition to offsetting emissions, REDD could provide indirect support for biodiversity conservation through reduced habitat loss, thus providing a unique solution to the longstanding tension between conservation interests and other land-use needs in tropical forest regions such as the Peruvian Amazon.

There are many challenges to making REDD work, and mapping forest carbon stocks and emissions at the high resolution demanded by investors and monitoring agencies remains a technical barrier. Satellite remote sensing offers a practical means to monitor forest cover (5, 6), but has not provided high-resolution estimates of carbon emissions (7). In contrast, field plots provide effective localized estimates of forest carbon stocks, but natural variation in forest carbon density may render plot-based approaches ineffective for estimating carbon over large areas. Furthermore, although plot-based studies are needed for long-term monitoring of forest dynamics, they are time-consuming and are usually placed to avoid land-use change, which is the main anthropogenic factor responsible for carbon flux to the atmosphere in tropical forests. New approaches are critically needed to extend the role of field plots to capture regional variation and to bridge a major gap between field and satellite observations.

One new approach is airborne light detection and ranging (LiDAR), which, when used with field calibration plots, is capable of estimating aboveground forest carbon densities (in units of Mg C ha^{-1}) (8). However, airborne LiDAR has not been proven for carbon mapping of high diversity Amazon forests, and a key obstacle to large-scale use of LiDAR for REDD monitoring is its relatively high cost of operation and small geographic coverage. However, combined with a strategic use of satellite data, airborne LiDAR may yield cost-effective, high-resolution maps of forest carbon stocks and emissions (9). This potential has never been realized at large geographic scales that would be pertinent to an international REDD program.

Here we report on a study to apply a new multiscale, multitemporal method to analyze carbon stocks and emissions throughout 4.3 million ha of lowland Amazon forest in the Department of Madre de Dios, Peru, as a procedure for achieving national-scale REDD mapping while assessing determinants of biomass stocks at a large geographic scale. Although subnational within Peru, the study area is equivalent to twice that of Costa Rica's forests, and our study was designed with a survey size that is logistically easy to implement multiple times to achieve necessary coverage for larger nations. The Madre de Dios region has undergone relatively moderate land-use change throughout the past century. However, paving of the Interoceanic Highway since 2006, along with new timber concessions and an influx of artisanal gold miners during the past 5 y, has rapidly increased land-use pressure. In this context, we sought to understand the sources of spatial and temporal variability in carbon stocks and emissions throughout this large and rapidly changing region of the Amazon basin. Our approach involves multiscale steps ranging from automated satellite mapping of deforestation and degradation to airborne LiDAR mapping to local-scale plot calibration measurements. The approach provides high-resolution maps of aboveground carbon densities and a retrospective mapping of carbon emissions based on current carbon densities and past forest cover changes (*SI Materials and Methods*).

Results and Discussion

Airborne LiDAR data yielded forest canopy height, underlying terrain, and canopy vertical profile, providing a comprehensive,

Author contributions: G.P.A. and G.V.P. designed research; G.P.A., G.V.P., J.M., D.E.K., J.K.C., J.J., T.K.-B., G.P.-A., E.V., L.S., M.V., and R.F.H. performed research; G.P.A., J.M., D.E.K., J.K.C., J.J., T.K.-B., and A.B. analyzed data; and G.P.A. and J.M. wrote the paper.

The authors declare no conflict of interest.

This article is a PNAS Direct Submission.

Freely available online through the PNAS open access option.

[1]To whom correspondence should be addressed. E-mail: gpa@stanford.edu.

This article contains supporting information online at www.pnas.org/lookup/suppl/doi:10.1073/pnas.1004875107/-/DCSupplemental.

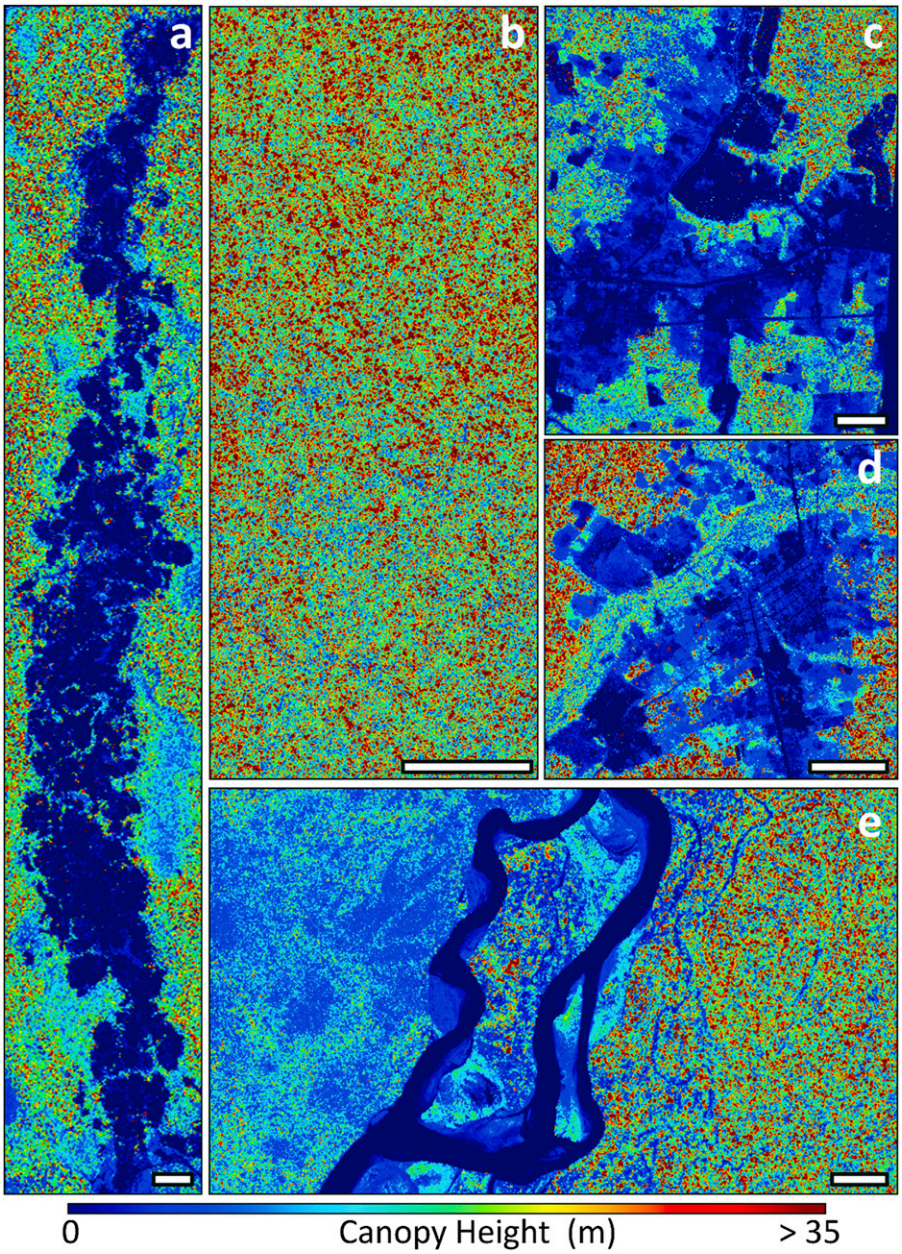

Fig. 1. Sources of variation in forest canopy height detected with high-resolution Carnegie Airborne Observatory LiDAR in the Peruvian Amazon: (*A*) artisanal gold mining; (*B*) selective logging; (*C*) deforestation for cattle ranching; (*D*) infrastructural development in towns, cities, and supporting land uses; and (*E*) alluvial and geologic substrate. White bars indicate a distance of 0.5 km in each example image.

regional inventory of both human-mediated and natural variation in Amazon forest canopy structure. Snapshot areas of 8,000 to 50,000 ha in size are shown in Fig. 1, each indicative of a major source of variation in canopy structure and carbon stocks throughout the region. Gold mining spans large areas of lowland swamp forest, leaving bare surface scars of up to 20 km in length with almost no remaining tree cover (Fig. 1*A*). Degradation from selective logging results in a spatially diffuse decrease in canopy height in otherwise intact forest (blue areas of Fig. 1*B*). Farming, cattle ranching (Fig. 1*C*), and infrastructural development (Fig. 1*D*) are major drivers of deforestation, leaving mosaics of depleted carbon stocks with diffusely scattered tree cover along roadways and in clearings. Finally, by virtue of being regional-scale, the data allowed us to assess gradients in forest structure mediated by geomorphic and fluvial processes (Fig. 1*E*).

During LiDAR overflights, a small, tactically placed network of field plots was established to convert LiDAR metrics of forest canopy structure to aboveground carbon density (Fig. S1). Extensive field validation, including both new and previously published estimates from field plots in the region (10, 11), indicated a LiDAR-to-carbon measurement correlation of 92% (Figs. S4–S6). Absolute mapping uncertainties were 23 Mg C ha^{-1} at 0.1 ha resolution, but decreased to just 5 Mg C ha^{-1}, or approximately 5% of the mean standing forest biomass stock, when the mapping results were integrated to 5 ha resolution (Figs. S7 and S8).

Application of LiDAR-based carbon statistics to forest type and condition maps derived from satellite data (*SI Materials and Methods*) yielded a 0.1-ha resolution map of aboveground carbon density throughout the 4.3 million ha region (Fig. 2). Total regional carbon storage was 395 Tg (million metric tons), and three

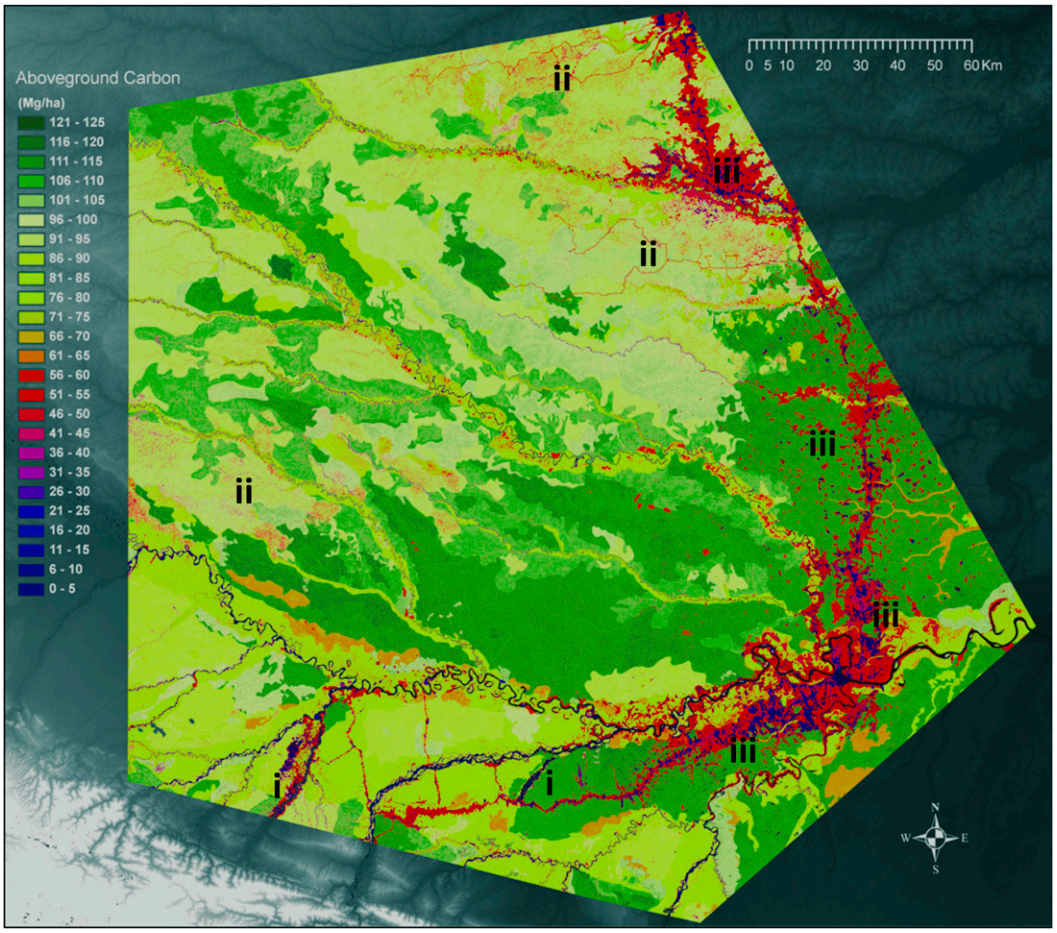

Fig. 2. Variation in aboveground carbon storage at 0.1 ha resolution throughout a 4.3 million ha region of the Peruvian Amazon, derived from an integrated use of CLASlite, LiDAR and field-plot data. Examples of (*i*) artisanal gold mining, (*ii*) selective logging and other forest disturbances, and (*iii*) deforestation for cattle ranching, road building, and other infrastructure are indicated.

major sources of variation in forest carbon were uncovered. First, we found a broad regional partitioning of standing carbon stocks mediated by geologic substrate (12, 13). To the north, older tertiary substrates support carbon densities with median values ranging from 85 to 100 Mg C ha^{-1}, whereas more fertile and flat Holocene alluvial surfaces in the central-east support 110 to 125 Mg C ha^{-1}. To the southwest, forests at the base of the Andes on Cretaceous surfaces maintain carbon densities in the range of 65 to 80 Mg C ha^{-1} (*t* test comparisons on randomly selected subsets, $P < 0.001$).

Stepping down in geographic scale from geologic controls, we uncovered enormous variation in standing carbon within and among forest types (Fig. 3*A* and Fig. S9). Median carbon density values were unique between forest types in most cases ($P < 0.001$; Fig. 2), but the highly varying distributions were the most revealing of ecological controls (Fig. 3*A*). Upland *terra firme* forests on low hills maintain the highest and widest range of carbon stocks, whereas inundated swamp areas with often monotypic palm cover are confined to a lower and narrower range of carbon storage conditions. Still wetter swamp forests with a dense shrub layer harbor even lower and narrower distributions of carbon. Areas that undergo periodic disturbance, such as floodplain forests and river edges, have highly skewed, multimodal distributions of carbon density, indicating a patch mosaic of distinct successional states. Finally, areas codominated by hardwood species and bamboo also show a bimodal distribution of carbon states.

Against this backdrop of geological and ecological control on carbon storage, the most pronounced, localized sources of carbon variation are deforestation, degradation, and secondary regrowth (Fig. 2). Although only 5% in geographic extent (Table 1), artisanal mine sites contain the lowest carbon densities among all land-use scenarios, just 16.7 ± 18.3 (SD) Mg C ha^{-1}. Selective logging and other forms of forest degradation are common, especially to the north, and account for 27% of the pixel-by-pixel changes in forest cover during the study period (Table 1). Forest degradation is diffusely distributed over large areas, but the individual pixels impacted within these areas support carbon stocks of only 35.6 ± 15.4 Mg C ha^{-1}, which is approximately 70% lower than background forest levels. Deforestation accounted for nearly 68% of forest loss throughout the region from 1999 to 2009. However, we found that deforestation results in a wide range of residual carbon stocks on the land: areas averaging 20% tree cover maintain 15.9 ± 32.8 Mg C ha^{-1}, whereas those maintaining at least 60% cover support 61.4 ± 56.2 Mg C ha^{-1} (Fig. S10).

Integrating historical deforestation and degradation results (Figs. S2 and S3) with 2009 carbon stocks (Fig. 2), we calculated annual gross aboveground carbon emissions from 1999 to 2009 (Fig. 3*B*). Results show a baseline emission rate for 1999 to 2006 of 0.26 ± 0.08 Tg C yr^{-1} from deforestation and 0.11 ± 0.02 Tg C yr^{-1} from degradation, for a sum of 0.37 Tg C yr^{-1}. Paving of the Interoceanic Highway since 2006, combined with new timber logging concessions and gold mining, caused an increase in deforestation emissions by more than 61% to 0.42 ±0.21 Tg C yr^{-1},

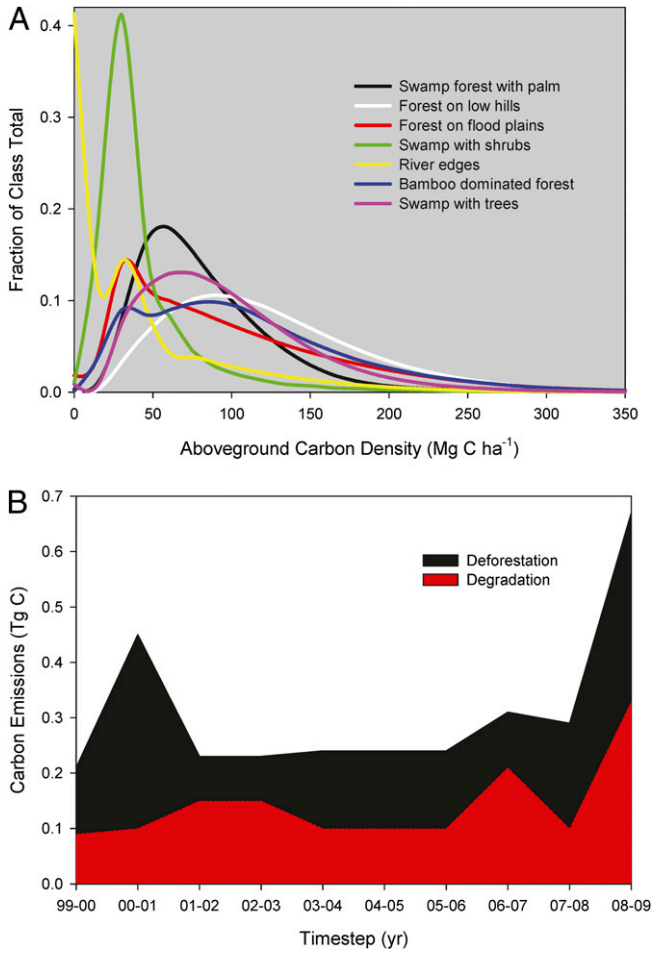

Fig. 3. (*A*) Distributions of aboveground carbon storage for the seven common forest types found in the Peruvian Amazon, derived from airborne LiDAR. (*B*) Annual emissions of carbon from deforestation and degradation mapped from time-series CLASlite imagery and LiDAR data.

whereas degradation emissions doubled to 0.21 ± 0.11 Tg C yr^{-1} (Fig. 3*B*). Critically, we found that degradation emissions averaged 47% of deforestation emissions (annual range, 22%–68%) during the 11-y study period, both before and during the recent increase in human activity throughout the region. In total, 4.529 Tg of aboveground carbon were committed to the atmosphere from 1999 to 2009, representing approximately 1.1% of the standing stock of forest carbon in the region.

Secondary forest regrowth, defined here as forests reestablished following any deforestation and degradation that occurred between 1999 and 2008, covered 24,823 ha in the study region, representing 38% of the total human-affected area by 2009 (Table 1). Forest regrowth resulted in a range of carbon densities (24-44 Mg C ha^{-1}) based on forest ages of 2 to 11 y (*SI Materials and Methods*). Nonetheless, the carbon density of secondary forest is 30.6 ± 16.7 Mg C ha^{-1}, or approximately 60% to 70% lower than the average carbon stocks for intact forests in the region. Integrated over the 11-y study period, secondary regrowth accumulated 0.812 Tg C, providing an 18% offset to gross emissions that resulted in a net regional loss of 3.717 Tg C to the atmosphere.

Our results uncover multiple spatial scales of variation in carbon stocks throughout the region, and change our understanding of how forest carbon is distributed and subsequently altered by land-use change in the southwestern Amazon. To our knowledge, this is the first study to detail regional-level variation in forest carbon densities mediated by geologic substrate and forest type (Figs. 2 and 3*A*). We also detected an interaction between geological controls on carbon storage and land-use effects on carbon emissions: deforestation emissions dominated the flatter quaternary substrates that are easier to access for road-building and farming. In contrast, degradation emissions from selective logging occurred mostly on eroded tertiary surfaces that are topographically dissected and difficult to access (Fig. 2).

The observed trend of increasing carbon emissions since 2006 following the development of the Interoceanic Highway is previously unmeasured (Fig. 3*B*), but more revealing is the large contribution of degradation to the total annual gross emissions for the region. Degradation added an average of 47% more carbon to the atmosphere than did deforestation alone, and increased in step with deforestation during the recent period of heightened land-use activity in the region. Degradation is diffusely distributed throughout the forested landscapes of Amazonia and other tropical regions, and only by combining very high-resolution airborne LiDAR techniques with large-area satellite mapping can these emissions be quantified and monitored over time.

The detailed statistical distributions of aboveground carbon density were also previously unmeasured because the majority of the region remains inaccessible on the ground. However, our airborne measurements reveal highly skewed, often multimodal, distributions of forest carbon. As a result, we contend that samples of forest carbon storage obtained with field plots, cannot account for the spatial variation in carbon stocks, especially in the context of the mosaic of anthropogenic land uses and resulting carbon emissions.

In support of REDD, the Intergovernmental Panel on Climate Change (IPCC) (14) issued a default tier-I estimation approach of forest carbon density based on average carbon values assigned for biomes. Applying the IPCC tier-I method to our study region produced an estimated 587 Tg C in aboveground biomass, whereas our spatially explicit mapping indicated just 395 Tg C (Fig. 2). This difference results primarily from the fact that forest carbon densities are not homogeneous at a variety of scales. Although our regional carbon estimates are 33% lower than IPCC tier-I estimates, the high-resolution, verifiable nature of our ap-

Table 1. Area of new land use and forest regrowth integrated from 1999 to 2009

Land use	Total area, ha	Proportion of human-affected area, %	Mean (SD) carbon density, Mg C ha^{-1}
Gold mining	3,207	4.9	16.7 (18.3)
Forest degradation*	17,740	27.3	35.6 (15.4)
Deforestation†	43,933	67.7	27.8 (16.9)
Secondary regrowth‡	24,823	38.3	32.7 (7.5)

Mean aboveground carbon densities are reported for 2009.
*Forest degradation is dominated by selective logging in this region.
†Deforestation is dominated by clearing for cattle ranching and farming in this region.
‡Regrowth calculated from deforestation and disturbance mapped between 1999 and 2008.

proach would likely yield increased investment per unit of carbon (15, 16). At the national scale, most tropical countries will rely initially on tier-I methods, which will generate large uncertainties and lower confidence, and thus potentially lower carbon credits (4, 15, 17). Developing monitoring capacities at higher accuracies—using procedures like those demonstrated here—will ultimately provide increased carbon credit, boosted carbon sequestration, and improved biodiversity protection.

The cost to implement this method of high-resolution carbon stock and emissions monitoring is decreasing. Satellite data costs are decreasing, and the major data sources are now free of charge to end users. The cost for analyzing the satellite data for forest cover, deforestation and degradation is also rapidly diminishing. The Carnegie Institution is making its Landsat Analysis System Lite (CLASlite) available for free to noncommercial organizations throughout the Amazon region (http://claslite.ciw.edu). LiDAR is a powerful airborne imaging technology that, like aerial photography in the 1970s and 1980s, is rapidly expanding throughout the world for use across a range of environmental sectors. There are now many airborne LiDAR mapping companies operating in the Americas, Europe, Africa, Asia, Australia, and the Pacific (http://www.airbornelasermapping.com). For this 4.3 million ha analysis, the Carnegie Airborne Observatory (CAO) operated its LiDAR, processed the data, and provided maps of forest structure at a cost of less than $0.08/ha. More recent work in Madagascar has reduced the cost to approximately $0.06/ha, and there exists a strong economy-of-scale effect whereby larger-area projects prove far more cost effective than small-area analyses. This runs opposite to plot-level work, which increases in cost on a per-area basis.

Finally, the procedure tested here can be scaled up to the national level. We selected this particular 4.3 million ha area for a variety of scientific purposes. The results can be directly extrapolated with the addition of highly available satellite imagery and CLASlite, and with no additional airborne or ground-based work, to an area of approximately 60 million ha based on the range of forest types found in Peru. However, the uncertainty in the regional variation of carbon densities applied to such a full national-scale satellite map would be reduced with additional LiDAR sampling throughout the region. Here we have reported the results of high-resolution mapping of carbon stocks and emissions in the Amazon region, and the approach is being implemented by three western Amazon countries.

Materials and Methods

Our approach involves four steps: (*i*) regional mapping of vegetation type and condition (forest cover, deforestation, degradation, regrowth) using moderate-resolution satellite data; (*ii*) regionally stratified large-area sampling of vegetation canopy 3D structure using airborne LiDAR; (*iii*) conversion of LiDAR vegetation structural data to aboveground carbon density using LiDAR allometrics developed at a limited number of field plots; and (*iv*) integration of the satellite maps with the calibrated LiDAR data to set a regional, high-resolution baseline carbon estimate, and mapping of carbon emissions retrospectively and into the future.

Forest condition—including deforestation, degradation, and regrowth—was assessed using the CLASlite (18) satellite mapping system with 30-m Landsat imagery in nearly annual time steps from 1999 to 2009 (Figs. S1–S3). Field validation surveys indicated that 2009 deforestation, degradation, and secondary regrowth maps had errors of 0% to 1.2%, 1.9% to 6.4%, and 2.6% to 2.9%, respectively (Tables S1 and S2). A map partitioning the study area into 26 vegetation classes, combined with CLASlite results, was used to locate 27 LiDAR survey areas covering a total of 514,317 ha for collection at a spatial resolution of 1 m or less throughout the 4.3 million ha region (Fig. S1). The LiDAR data were collected using the CAO (19). Calibration and validation of the airborne- and satellite-based estimates of aboveground carbon density were carried out during the overflights. Detailed information on each of these steps is provided in *SI Materials and Methods*.

ACKNOWLEDGMENTS. We thank G. Agosti, M. E. Arroyo, L. Carranza, J. A. Escudero, A. Felix, A. Forsyth, N. Jarmillo, K. Ledesma, A. Mulanovich, R. E. Martin, C. Moran, J. C. Rivera, A. Rosenthal, and C. Verastegui for logistical and field assistance; T. Baker and the RAINFOR Network for providing field data for LiDAR validation work; and Bosque Sociedad y Desarrollo Institution, H. Duenas, the herbarium of the National University of Madre de Dios, the Protected Areas Natural Service (SERNANP), and especially the Amazon Conservation Association for logistical assistance. This project was supported by the Government of Norway, Gordon and Betty Moore Foundation, Carnegie Institution, W. M. Keck Foundation, and William Hearst III.

1. IPCC (2007) *Climate Change 2007: Impacts, Adaptation and Vulnerability* (Cambridge Univ Press, New York).
2. van der Werf GR, et al. (2009) CO2 emissions from forest loss. *Nat Geosci* 2:737–738.
3. Olander LP, Gibbs HK, Steininger M, Swenson JJ, Murray BC (2008) Reference scenarios for deforestation and forest degradation in support of REDD: A review of data and methods. *Environ Res Lett* 3:025011.
4. Angelsen A (2008) Moving Ahead with REDD: Issues, Options and Implications (Center for International Forestry Research, Bogor, Indonesia).
5. Hansen MC, et al. (2008) Humid tropical forest clearing from 2000 to 2005 quantified by using multitemporal and multiresolution remotely sensed data. *Proc Natl Acad Sci USA* 105:9439–9444.
6. Achard F, et al. (2007) Pan-tropical monitoring of deforestation. *Environ Res Lett* 2: 1–11.
7. Global Observation of Forest and Land Cover Dynamics (2008) *Reducing Greenhouse Gas Emissions From Deforestation and Degradation in Developing Countries: A Sourcebook of Methods and Procedures for Monitoring, Measuring and Reporting.* (Natural Resources Canada, Calgary, AB, Canada).
8. Lefsky MA, et al. (2002) Lidar remote sensing of above-ground biomass in three biomes. *Glob Ecol Biogeogr* 11:393–399.
9. Asner GP (2009) Tropical forest carbon assessment: Integrating satellite and airborne mapping approaches. *Environ Res Lett* 3:03009.
10. Phillips OL, et al. (1998) Changes in the carbon balance of tropical forests: Evidence from long-term plots. *Science* 282:439–442.
11. Anderson LO, et al. (2009) Influence of landscape heterogeneity on spatial patterns of wood productivity, wood specific density and above ground biomass in Amazonia. *Biogeosciences* 6:1883–1902.
12. Campbell KE, Jr, Heizler M, Frailey CD, Romero-Pittman L, Prothero DR (2001) Upper Cenozoic chronostratigraphy of the southwestern Amazon Basin. *Geology* 29:595–598.
13. Sombroek W (2000) Amazon landforms and soils in relation to biological diversity. *Acta Amazonica* 31:81–100.
14. Eggleston HS, Buendia L, Miwa K, Ngara T, Tanabe K, eds (2006) *2006 IPCC Guidelines for National Greenhouse Gas Inventories.* Intergovernmental Panel on Climate Change. (Institute for Global Environmental Strategies, Kanagawa, Japan).
15. Mollicone D, et al. (2007) Elements for the expected mechanisms on "Reduced Emissions from Deforestation and Degradation (REDD)" under UNFCCC. *Environ Res Lett* 2:045024.
16. Giacomo G, et al. (2008) Applying the conservativeness principle to REDD to deal with the uncertainties of the estimates. *Environ Res Lett* 3:035005.
17. Gibbs HK, Brown S, Niles JO, Foley JA (2007) Monitoring and estimating tropical forest carbon stocks: Making REDD a reality. *Environ Res Lett* 2:1–13.
18. Asner GP, Knapp DE, Balaji A, Paez-Acosta G (2009) Automated mapping of tropical deforestation and forest degradation: CLASlite. *J Appl Remote Sens* 3:033543.
19. Asner GP, et al. (2007) Carnegie Airborne Observatory: In-flight fusion of hyperspectral imaging and waveform light detection and ranging (LiDAR) for three-dimensional studies of ecosystems. *J Appl Remote Sens* 1:1–21.